Graph Wavelet Packets for the Classification of Brain Data in Anxiety and Depression

Sébastien Dam, Pierre Maurel, Julie Cologner

Graph Wavelet Packets for the Classification of Brain Data in Anxiety and Depression

Sébastien Dam, Pierre Maurel, Julie Coloigner
Univ Rennes, Inria, CNRS, Inserm, IRISA UMR 6074, Empenn ERL U 1228, F-35000 Rennes, France
Corresponding author: julie.coloigner@irisa.fr

***Abstract*—Recent research has been focusing on Graph Signal Processing (GSP) to combine different neuroimaging modalities, enabling the integration of both structural and functional brain data. To characterize how signals interact with brain networks, the Fourier and wavelet transforms have been extended to the graph setting by designing spectral filters on the structural graph Laplacian eigenvalues. Here, we present the benefits of leveraging graph wavelet packets in neuroimaging using diffusion MRI and fMRI data, based on the Boston Adolescent Neuroimaging of Depression and Anxiety (BANDA) dataset. We consider the distance between eigenvectors to extract features related to the spectral domain of the structural graph. Our proposed framework demonstrates superior accuracies in a classification scheme compared to conventional GSP methods.**

***Index Terms*—anxiety, depression, functional MRI, graph signal processing, structural connectivity, graph wavelet packets**

I. Introduction

Anxiety and depression in adolescents are mental health conditions that negatively affect the quality of life. Our knowledge of the biological mechanisms behind those diseases is still limited and the aim of this project is to improve our understanding of the cerebral underpinnings behind them.

Brain connectivity has been extensively studied for investigating clinical biomarkers of psychiatric diseases [1], [2]. Functional connectivity (FC) captures the similarity between brain regions by measuring the correlation between Blood-Oxygen-Level-Dependent (BOLD) signals, i.e., time-series extracted from resting-state functional Magnetic Resonance Imaging (rs-fMRI). Structural connectivity (SC) focuses on the anatomical connections between brain regions estimated by tractography techniques to provide insights into neural connectivity pathways and patterns. Many neuroimaging studies investigated FC and SC to provide a better understanding of psychiatric diseases in adults [3], [4]. Among them, several papers studied the structural-functional brain connectome of depression and reported disturbances in various brain networks in patients, such as the default mode network (DMN), frontoparietal network (FPN) and cingulo-opercular network [5]. Likewise, a recent review and meta-analysis of rs-fMRI revealed altered connectivity between the amygdala and the prefrontal regions in anxious patients [3]. Investigating youth depression and anxiety is also crucial because the emergence of treatment-resistance conditions often correlates with the diagnostic of these disorders during adolescence [6]. Yet, there is a lack of research studying markers in youth. The main meta-analyses found altered FC in the DMN, the FPN, and the salience network [7], [8].

While these results are meaningful, most of these studies analyzed different modalities independently. However, due to the intricate nature of the brain, integration of both structural and functional brain data is hypothesized to enable identification of more robust markers of brain diseases [9], [10]. Graph Signal Processing (GSP) is a promising framework in this respect. It uses the eigendecomposition of the structural graph Laplacian to unveil the topological organization of brain regions across various scales, enabling the examination of frequency patterns of SC. By defining the BOLD signals on the underlying graph structure, GSP helps uncover hidden relationships that might exist between these two modalities. Recent works studied the frequency behavior of the BOLD signals by computing their Graph Fourier Transform (GFT), which decomposes the signals into the spectral domain to reveal how they align with the global network topology of the structure. In [11], the superior predictive performance of using feature vectors derived from the GFT was shown in a supervised classification setting of autism, when compared to classical connectivity metrics extracted from FC or rs-fMRI time-series alone. GFT coefficients were also used to analyze the coupling strengths between rs-fMRI time-series and SC with low- or high-pass filters in the context of classification of patients with disorders such as depression [12], anxiety [13], and Alzheimer's disease [14].

With the development of GSP, there have been several attempts to derive wavelets on graphs by building spectral filters on the Laplacian eigenvalues [15], [16]. Specifically, the Spectral Graph Wavelet Transform (SGWT) maps graph signals to coefficients and enables localization on both the spatial node and spectral domains [17]. However, whether it is with the GFT or SGWT, previous studies exclusively focused on the eigenvalues to organize the corresponding eigenvectors. Therefore, the relationships among the latest have been neglected. In this work, we propose an alternative strategy, that is, to make use for the first time of the direct distances between graph Laplacian eigenvectors in neuroimaging. We create a new set of graph transforms that aims to extend previous transforms by fully leveraging the graph structure, which enables a better localization on the spatial and spectral domains. The proposed approach is evaluated in a classification setting to predict anxiety and depression, and is compared to the features obtained with the GFT and SGWT.

II. Preliminaries

A. Data

The BANDA study is one of the projects funded by the National Institute of Health to study a disease population using Human Connectome Project protocols [18]. This cohort includes 207 adolescents with brain imaging data (62 Control (CA), 80 Anxious (AA) and 65 Depressed Adolescents (DA)). We discarded 17 subjects due to poor image quality, resulting in $N_s = 190$ subjects including 58 CA, 72 AA and 60 DA. Three modalities of brain imaging data (structure MRI, rs-fMRI and diffusion-weighted images) were acquired for each participant.

B. Preprocessing

The data were preprocessed using QSIPrep [19] and fMRIPrep [20]. The anatomical preprocessing workflows contain intensity non-uniformity correction of the T1w image, skull-stripping, and brain tissue segmentation of cerebrospinal fluid, white-matter and gray-matter. The diffusion-weighted images were denoised using MP-PCA, then corrected for Gibbs unringing using local subvoxel-shifts, B1 field inhomogeneity using ANT's N4 algorithm, head motion and Eddy current using FSL's eddy. For fMRI images, head-motion parameters (transformation matrices and six corresponding rotation and translation parameters) were estimated using FSL's mcflirt. A fieldmap was estimated based on two echo-planar imaging references with opposing phase-encoding directions, with FSL's topup. BOLD runs were also slice-time corrected using 3dTshift from AFNI. Finally, the brain parcellation Schaefer atlas with 400 cortical regions [21] and 16 subcortical regions [22] was adopted to construct SC matrices and extract BOLD signals of all voxels within the regions of interest (ROIs) according to the template. Whole brain probabilistic tractography including 10 million fibers was performed, using a spherical deconvolution approach and the Spherical-deconvolution Informed Filtering of Tractograms 2 [23].

C. Graph Signal Processing

Let $\mathcal{G} = \mathcal{G}(\mathcal{V}, \mathcal{E}, \boldsymbol{A})$ be an undirected graph representing the SC, where $\mathcal{V}$ is the set of nodes with each node representing a distinct ROI, $\mathcal{E}$ is the set of undirected edges in $\mathcal{G}$, and $\boldsymbol{A}$ is a symmetric weighted matrix representing the adjacency matrix where each entry is the number of fibers that link two ROIs. Let $\boldsymbol{X} \in \mathbb{R}^{N \times T}$ be the BOLD signals for N ROIs over the course of T timepoints. We can now define the combinatorial Laplacian matrix, random-walk normalized normalized Laplacian matrix and the symmetric normalized Laplacian matrix, respectively as

$$\begin{aligned} \boldsymbol{L} &= \boldsymbol{D} - \boldsymbol{A} \\ \boldsymbol{L}_{\text{rw}} &= \boldsymbol{D}^{-1}\boldsymbol{L} \\ \boldsymbol{L}_{\text{sym}} &= \boldsymbol{I} - \boldsymbol{D}^{-1/2}\boldsymbol{A}\boldsymbol{D}^{-1/2}, \end{aligned} \tag{1}$$

where $\boldsymbol{D}$ is the diagonal matrix of node degrees, i.e., $\boldsymbol{D}_{ii} = \sum_j \boldsymbol{A}_{ij}$. $\boldsymbol{L}_{\text{sym}}$ is widely used in graph theory. Since it is real, symmetric, and positive semi-definite, it can be diagonalized via its eigendecomposition as $\boldsymbol{L}_{\text{sym}} = \boldsymbol{U}\boldsymbol{\Lambda}\boldsymbol{U}^\top$, where the columns of $\boldsymbol{U} = [u_1, u_2, \ldots, u_N]$ are the orthonormal eigenvectors, and $\boldsymbol{\Lambda}$ is the diagonal matrix that stores the non-negative eigenvalues $\boldsymbol{\Lambda} = diag(\lambda_1, \lambda_2, \ldots, \lambda_N)$. Each eigenvalue λ_k reflects a notion of frequency of the corresponding eigenvector u_k, which can be interpreted as a structural harmonic. The BOLD signals $\boldsymbol{X}$ can then be projected on the structural harmonics through the GFT to perform a frequency analysis of the graph signals, as defined below:

$$\hat{\boldsymbol{X}} = \boldsymbol{U}^\top \boldsymbol{X}. \tag{2}$$

D. Graph Wavelet Transform

The GFT can be further exploited to construct graph wavelets that are localized both in the spatial and spectral domains, which is not the case for the GFT coefficients that are only localized in the latest. In [17], the SGWT was introduced to build wavelet frames adapted on graphs as $\boldsymbol{\psi}_{j,n} = \boldsymbol{U}g(j\boldsymbol{\Lambda})\boldsymbol{U}^\top\delta_n$, where g is a band-pass kernel defined in the spectral domain, j is the scale parameter and δ_n is the standard basis vector centered at node n. A low-pass filter or scaling function $h(\lambda)$ is added to compute the complete frame. The scale parameter j and the position parameter n provide the ability to examine the spatial and spectral domains at different levels of localization and scale. Therefore, the wavelet coefficients of a given graph signal $\boldsymbol{X}$ are obtained by computing the following inner product:

$$\boldsymbol{W}(j, n) = \langle \boldsymbol{\psi}_{j,n}, \boldsymbol{X} \rangle. \tag{3}$$

We now explain in an intuitive example how the exclusive use of the eigenvalues to build filters for the GFT and SGWT may be limited to fully exploit the graph structure. As represented in Figure 1, the first six eigenvectors ordered sequentially in terms of increasing eigenvalues oscillate in different directions. As the frequencies increase, the smoothness in terms of values between neighboring ROIs decrease accordingly. This representation enables the construction of filters for graph signals. However, these filters depend only on the 1D sequence of eigenvalues, and do not reflect how the eigenvectors behave. This is illustrated between the second and third eigenvector, where the type of oscillations is completely different, despite the values of the associated frequencies being

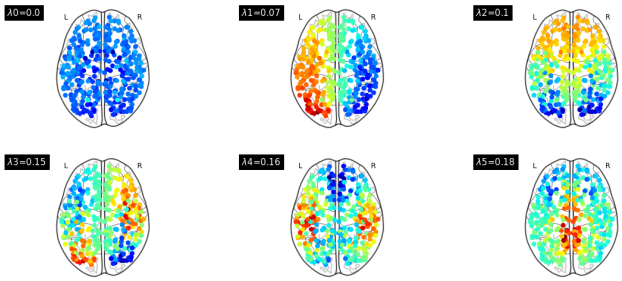

Fig. 1. The first six Laplacian eigenvectors.

close to each other. In other words, the spatial information given by the eigenvectors is completely overlooked by simply taking the eigenvalue sequence into account.

III. Methods

We propose to construct well localized basis vectors based on the eigenvectors, which will allow to build discriminative features in the graph spectral domain. Our approach is detailed in the following subsections.

A. Natural distance between eigenvectors

We first introduce a pseudometric that quantifies the difference between the eigenvectors using the Difference of Absolute Gradient (DAG) pseudometric [24]. To incorporate information related to the oscillations of the eigenvectors, their gradient on each edge is first computed. Due to the undirected nature of $\mathcal{G}$, the absolute value of the gradients is considered. Then, the distance between the eigenvectors is computed using these values with the l^2-distance. Therefore, eigenvectors with similar oscillation patterns are expected to output a small DAG distance, while those with different oscillations would lead to a large DAG distance. Let $\boldsymbol{Q} \in \mathbb{R}^{N\times|\mathcal{E}|}$ be the incidence matrix of $\mathcal{G}$, defined as

$$\boldsymbol{Q}_{i,k} = \begin{cases} -\sqrt{\boldsymbol{A}_{i,j}} & \text{if } e_k = (v_i, v_j) \text{ for some } j, \\ +\sqrt{\boldsymbol{A}_{i,j}} & \text{if } e_k = (v_j, v_i) \text{ for some } j, \\ 0 & \text{otherwise,} \end{cases} \tag{4}$$

where $v_i \in \mathcal{V}$ is a node and $e_k = (v_i, v_j) \in \mathcal{E}$ is an edge from v_i to v_j. The matrix $\boldsymbol{Q}$ verifies $\boldsymbol{Q}\boldsymbol{Q}^T = \boldsymbol{L}$.

Then, the DAG pseudometric between u_i and u_j is defined as

$$\begin{aligned} d_{\text{DAG}}(u_i, u_j) &= \||\nabla_G|u_i - |\nabla_G|u_j\|_2 \\ \text{where } |\nabla_G|u &= \text{abs}(\boldsymbol{Q}^T u) \in \mathbb{R}^N_{\geq 0}, \end{aligned} \tag{5}$$

where abs(.) applies the absolute value to its argument. For further details related to the properties of this pseudometric, see [25]. Now that the difference between eigenvectors has been quantified, we can use it to build graph wavelet packets.

B. Natural graph wavelet packets

Instead of relying on the eigenvalue sequence to build filters, we conduct an approach as proposed in [25], which allows to construct a graph wavelet packet dictionary of well localized vectors. This construction is achieved in two steps that are explained in the following subsections.

1) Hierarchical bipartition of eigenvectors: Let $\mathcal{G}^* = \mathcal{G}^*(\mathcal{V}^*, \mathcal{E}^*, \boldsymbol{A}^*)$ be the dual graph of $\mathcal{G}$, where the set of eigenvectors $\mathcal{V}^* = \{u_1, u_2, \ldots, u_n\}$ are the nodes, $\mathcal{E}^*$ is the set of undirected edges, and $\boldsymbol{A}^*_{i,j} = 1/d_{\text{DAG}}(u_{i-1}, u_{j-1})$, $\forall i, j = 1, 2, \ldots, N$. We chose $\mathcal{V}^*$ as the set of eigenvectors of the combinatorial Laplacian. The main advantage of considering this dual graph is that we can fully study the relations between the eigenvectors in a complete graph setting, which brings clearly more specific patterns of the brain structure than simply using the eigenvalue magnitudes [25]. Therefore, we can construct a graph wavelet packet dictionary by bipartitioning $\mathcal{G}^*$ recursively via spectral graph bipartitioning using the Fiedler vectors of $\boldsymbol{L}_{\text{rw}}$ (see 1), whose use is preferred compared to $\boldsymbol{L}$ or $\boldsymbol{L}_{\text{sym}}$ in the case of graphs where node degrees are widely distributed [26]. At each level j, there are 2^j subgraphs and bipartitioning is performed on each of these subgraphs to obtain the bipartition at level $j+1$. Increasing the level j of the bipartition thus corresponds to a more localized basis vector in $\mathcal{G}$.

2) Localization on $\mathcal{G}$ via varimax rotation: After the construction of the hierarchical bipartition, the varimax rotation is performed on the eigenvectors of each subgraph of $\mathcal{G}^*$ at a given level j. Let $\boldsymbol{U}_k^{(j)} \in \mathbb{R}^{N\times N_k^j}$ be a matrix whose columns are the eigenvectors belonging to $\mathcal{V}_k^{*(j)}$, where j is the level in the bipartition, and N_k^j is the number of eigenvectors at level j in the k-th subgraph. Applying the varimax rotation to $\boldsymbol{U}_k^{(j)}$ consists in adjusting the orientation of its columns, such that the variances of the squared values of the columns are maximized. Due to the orthonormality of the columns of $\boldsymbol{U}_k^{(j)}$, this operation is equivalent to an orthogonal rotation that maximizes the overall 4-th order moments, i.e.,

$$\boldsymbol{\Psi}_k^{(j)} = \boldsymbol{U}_k^{(j)} R_k^{(j)}, \tag{6}$$

where $R_k^{(j)} = \underset{R\in\text{SO}(N_k^j)}{\arg\max} \sum_{p=1}^{N}\sum_{q=1}^{N_k^j} \left[\left(\boldsymbol{U}_k^{(j)} R\right)^4\right]_{p,q}$. In other words, this rotation acts as an approximate entropy minimizer of the distribution of the columns of $\boldsymbol{U}_k^{(j)}$ [27], which thus outputs column vectors that are more localized in $\mathcal{G}$ than those of $\boldsymbol{U}_k^{(j)}$. We refer to the dictionary $\{\boldsymbol{\Psi}_k^j\}_{j=0:J;k=0:2^j-1}$ as the Varimax Natural Graph Wavelet Packet (VM-NGWP) dictionary.

C. Classification

Now that we have obtained well localized basis vectors that are ordered according to the natural distance between the eigenvectors, we can concatenate them into a single matrix $\boldsymbol{\Psi}^{(j)} \in \mathbb{R}^{N\times N}$ for each level j to project the BOLD signals $\boldsymbol{X}$:

$$\boldsymbol{Y}^{(j)} = \langle \boldsymbol{\Psi}^{(j)}, \boldsymbol{X} \rangle. \tag{7}$$

This projection can be interpreted as filtering of BOLD signals by natural localized vectors. We note that the eigenvectors were computed for each SC to take into account individual variability. The VM-NGWP dictionary was constructed for multiple levels j ranging from 2 to 9, thus outputting 8 feature vectors of dimension $N_s \times N$ after projection. To account for the potential redundancy and complementarity of the projected data, we conducted a principal component analysis on the concatenated set of feature vectors across subjects and ROIs using the tidy data standard [28]. The first principal components that explained 80% of the variability were then extracted and used as input for the classification task. Classification was performed by training a linear support

vector machine (SVM) model with parameter $C = 0.1$ in a cross-validation scheme with a train-test split of 90/10%, using a stratified shuffle over 50 splits. Other models such as the SVM with the radial basis function kernel or the logistic regression were tested, along with an optimal search for the different hyperparameters, but the linear SVM gave the best performances. Incremental feature selection was carried out on the ROIs by starting classification with a small subset of features and iteratively adding additional features to the subset in increments of 10 at each step. At each iteration, the features were ranked via ANOVA and the classification was performed until all features (N) were considered.

The classification performance of our framework (that we refer simply as VM-NGWP) was compared with two other methods: based on the classification of (i) GFT coefficients and (ii) SGWT coefficients (cf. Sec. II-C, II-D).

- For the GFT coefficients, we computed their variance using the full frequency bands, and for different frequency bands given the low, middle and high frequency modes, called GFT, GFT_{LOW} GFT_{MID}, GFT_{HIGH}, respectively. These bands were defined by splitting the spectral domain into three portions with equal energy, based on average energy spectral density (across time) for each subject.
- For the SGWT coefficients, referred as SGWT, we chose Itersine as the filter bank of wavelets, which is a tight frame that covers a large part of the spectrum [29].

IV. Results and Discussion

Table I shows the averaged test accuracies of the splits. The best average accuracy for the classification of CA and DA was obtained for our framework, showing that considering the distances between eigenvectors to construct natural spectral filters improves prediction in depression. For the prediction of anxiety, while SGWT gives the best accuracy by a slight margin compared to our framework, we observe that these two methods outperform those based on GFT coefficients. This suggests that localized basis vectors may help obtaining more discriminative features. Moreover, except for the VM-NGWP dictionary, the overall accuracies are higher for the prediction of anxiety compared to depression. This suggests that our framework may be more robust for diseases with greater heterogeneity in the phenotypes than the other methods.

Figure 2 depicts the accuracies of the different methods used for the classification of CA and DA, as a function of the number of features. The best classification accuracy was obtained for our framework, with a gain of approximatively 8%. In comparison with the GFT and wavelet coefficients, our results show that relying only on the eigenvalues to build the projectors for the graph signals is not sufficient and complex spatial patterns information given by the eigenvectors may instead provide more valuable discriminative features. Indeed, the accuracies obtained based on the features from the GFT or SGWT coefficients struggle to exceed the baseline of 50%.

In Figure 2, we observe that at around 150 features, the accuracy obtained with the VM-NGWP dictionary starts reaching a plateau. Therefore, we select this number of features to

TABLE I
Comparison of averaged test accuracies. AA: Anxious Adolescents; CA: Control Adolescents; DA: Depressed Adolescents.

Methods	CA vs. AA (%)	CA vs. DA (%)
GFT	55.2	54.7
GFT_{LOW}	55.1	55.7
GFT_{MID}	53.8	49.5
GFT_{HIGH}	56.3	50.3
SGWT	**59.0**	54.9
VM-NGWP	58.0	**63.3**

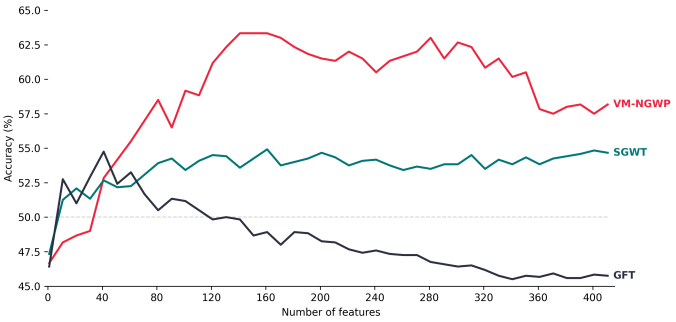

Fig. 2. Comparison of classification accuracies between control and depressed adolescents across increasing numbers of features.

retrieve the ROIs that were the most predictive. Figure 3 depicts the different scale and spatial localizations of the largest SVM coefficients that best separate the DA from the CA. The top features include several ROIs from the FPN such as the precuneus and the orbitofrontal cortex, the DMN with the parietal and prefrontal cortices, and the salience/ventral attention network (SVAN). Those networks have been linked with depression as they are involved in processes like attentional control, rumination and emotion regulation. For example, the FPN and DMN have been extensively studied in relation to depression, depicting altered connectivity within key regions of those networks such as the ones we found, and related to deficits in cognitive control and regulating mood [30]. Likewise, the presence of regions from the SVAN is consistent with previous studies, as they can be related to difficulties in regulating emotions and shifting attention appropriately in adolescents, such that altered connectivity in the SVAN may ultimately constitute a risk factor for developing a new onset of a depressive disorder [31].

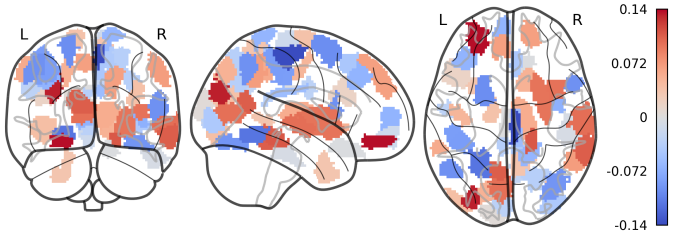

Fig. 3. Scale-Localization map of the best SVM coefficients on the brain for the classification of control and depressed adolescents.

V. Conclusion

In this paper, we proposed a framework to classify anxious and depressed adolescents using graph wavelet packets. In most multimodal approaches that use GSP, the major features are extracted based on the structural graph Laplacian eigenvalues. Here, we considered the relationships among eigenvectors to fully leverage the graph structure and build well localised basis vectors. Through comparative experiments, the results demonstrate the effectiveness of our framework as it showed the highest average accuracy in the classification of depression and performed relatively well for anxiety. In future work, we plan to examine how our approach could be combined with deep learning on graphs to further enhance classification performances.

Acknowledgment

Data and/or research tools used in the preparation of this manuscript were obtained from the National Institute of Mental Health (NIMH) Data Archive (NDA). NDA is a collaborative informatics system created by the National Institutes of Health to provide a national resource to support and accelerate research in mental health. Dataset identifier(s): 10.15154/3tk5-pb47. This manuscript reflects the views of the authors and may not reflect the opinions or views of the NIH or of the Submitters submitting original data to NDA.

References

[1] V. Menon, "Large-scale brain networks and psychopathology: a unifying triple network model," *Trends in Cognitive Sciences*, 2011.

[2] A. Fornito and B. Harrison, "Brain connectivity and mental illness," *Frontiers in Psychiatry*, vol. 3, 2012.

[3] A. Zugman, L. Jett, C. Antonacci, A. M. Winkler, and D. S. Pine, "A systematic review and meta-analysis of resting-state fmri in anxiety disorders: Need for data sharing to move the field forward," *Journal of Anxiety Disorders*, vol. 99, p. 102773, 2023.

[4] S. Ayyash, A. Davis, G. Alders, G. MacQueen, S. Strother, S. Hassel, M. Zamyadi, S. Arnott, J. Harris, R. Lam, R. Milev, D. J. Mueller (Müller), S. Kennedy, S. Rotzinger, B. Frey, L. Minuzzi, and G. Hall, "Exploring brain connectivity changes in major depressive disorder using functional-structural data fusion: A can-bind-1 study," *Human Brain Mapping*, vol. 42, 2021.

[5] J.-C. Roy, T. Desmidt, S. Dam, I. Mirea-Grivel, L. Weyl, E. Bannier, L. Barantin, D. Drapier, J.-M. Batail, R. David, J. Coloigner, and G. Robert, "Connectivity patterns of the core resting-state networks associated with apathy in late-life depression," *Journal of Psychiatry and Neuroscience*, vol. 48, pp. E404–E413, 2023.

[6] V. Dunn and I. M. Goodyer, "Longitudinal investigation into childhood- and adolescence-onset depression: psychiatric outcome in early adulthood," *The British Journal of Psychiatry*, 2006.

[7] R. Kerestes, C. G. Davey, K. Stephanou, S. Whittle, and B. J. Harrison, "Functional brain imaging studies of youth depression: A systematic review," *NeuroImage: Clinical*, vol. 4, pp. 209–231, 2014.

[8] J. Xu, N. T. Van Dam, C. Feng, Y. Luo, H. Ai, R. Gu, and P. Xu, "Anxious brain networks: A coordinate-based activation likelihood estimation meta-analysis of resting-state functional connectivity studies in anxiety," *Neuroscience & Biobehavioral Reviews*, vol. 96, pp. 21–30, 2019.

[9] J. Zhao, C.-C. Huang, Y. Zhang, Y. Liu, S.-J. Tsai, and C.-Y. Lo, "Structure-function coupling in white matter uncovers the abnormal brain connectivity in schizophrenia," *Translational psychiatry*, 2023.

[10] X. Xu, S. Xu, L. Han, and X. Yao, "Coupling analysis between functional and structural brain networks in alzheimer's disease," *Mathematical Biosciences and Engineering*, 2022.

[11] A. Brahim and N. Farrugia, "Graph fourier transform of fmri temporal signals based on an averaged structural connectome for the classification of neuroimaging," *Artificial Intelligence in Medicine*, 2020.

[12] P. J. Thomas, A. Leow, H. Klumpp, K. L. Phan, and O. Ajilore, "Default mode network hypoalignment of function to structure correlates with depression and rumination," *Biological Psychiatry: Cognitive Neuroscience and Neuroimaging*, vol. 9, no. 1, pp. 101–111, 2024.

[13] G. Orrù, P. Maurel, and J. Coloigner, "Structural and functional interplay in anxiety related classification: A graph signal processing approach," in *2021 IEEE 18th International Symposium on Biomedical Imaging (ISBI)*, 2021, pp. 271–274.

[14] H. Padole, S. Joshi, and T. K. Gandhi, "Early detection of alzheimer's disease using graph signal processing on neuroimaging data," in *2018 2nd European Conference on Electrical Engineering and Computer Science (EECS)*, 2018, pp. 302–306.

[15] R. R. Coifman and M. Maggioni, "Diffusion wavelets," *Applied and Computational Harmonic Analysis*, 2006, special Issue: Diffusion Maps and Wavelets.

[16] I. M. Bulai and S. Saliani, "Spectral graph wavelet packets frames," *Applied and Computational Harmonic Analysis*, 2023.

[17] D. K. Hammond, P. Vandergheynst, and R. Gribonval, "Wavelets on graphs via spectral graph theory," *Applied and Computational Harmonic Analysis*, vol. 30, no. 2, pp. 129–150, 2011.

[18] V. Siless, N. A. Hubbard, R. Jones, J. Wang, N. Lo, C. C. Bauer, M. Goncalves, I. Frosch, D. Norton, G. Vergara, K. Conroy, F. V. De Souza, I. M. Rosso, A. H. Wickham, E. A. Cosby, M. Pinaire, D. Hirshfeld-Becker, D. A. Pizzagalli, A. Henin, S. G. Hofmann, R. P. Auerbach, S. Ghosh, J. Gabrieli, S. Whitfield-Gabrieli, and A. Yendiki, "Image acquisition and quality assurance in the boston adolescent neuroimaging of depression and anxiety study," *NeuroImage: Clinical*, vol. 26, p. 102242, 2020.

[19] M. Cieslak, P. Cook, X.-S. He, F.-C. Yeh, T. Dhollander, A. Adebimpe, G. Aguirre, D. Bassett, R. Betzel, J. Bourque, L. Cabral, C. Davatzikos, J. Detre, E. Earl, M. Elliott, S. Fadnavis, D. Fair, W. Foran, P. Fotiadis, and T. Satterthwaite, "Qsiprep: an integrative platform for preprocessing and reconstructing diffusion mri data," *Nature Methods*, 2021.

[20] O. Esteban, C. J. Markiewicz, R. W. Blair, C. A. S. Moodie, A. I. Isik, A. Erramuzpe, J. D. Kent, M. Goncalves, E. Dupre, M. Snyder, H. Oya, S. S. Ghosh, J. Wright, J. Durnez, R. A. Poldrack, and K. J. Gorgolewski, "Fmriprep: a robust preprocessing pipeline for functional mri," *Nature methods*, vol. 16, pp. 111 – 116, 2018.

[21] A. Schaefer, R. Kong, E. M. Gordon, T. O. Laumann, X.-N. Zuo, A. J. Holmes, S. B. Eickhoff, and B. T. T. Yeo, "Local-Global Parcellation of the Human Cerebral Cortex from Intrinsic Functional Connectivity MRI," *Cerebral Cortex*, vol. 28, no. 9, pp. 3095–3114, 2017.

[22] Y. Tian, D. S. Margulies, M. Breakspear, and A. Zalesky, "Topographic organization of the human subcortex unveiled with functional connectivity gradients," *Nature Neuroscience*, 2020.

[23] R. E. Smith, J.-D. Tournier, F. Calamante, and A. Connelly, "Sift2: Enabling dense quantitative assessment of brain white matter connectivity using streamlines tractography," *NeuroImage*, vol. 119, pp. 338–351, 2015.

[24] H. Li and N. Saito, "Metrics of graph Laplacian eigenvectors," in *Wavelets and Sparsity XVIII*, D. V. D. Ville, M. Papadakis, and Y. M. Lu, Eds., vol. 11138, International Society for Optics and Photonics. SPIE, 2019, p. 111381K.

[25] A. Cloninger, H. Li, and N. Saito, "Natural graph wavelet packet dictionaries," *Journal of Fourier Analysis and Applications*, vol. 27, 2021.

[26] U. Luxburg, "A tutorial on spectral clustering," *Statistics and Computing*, vol. 17, pp. 395–416, 2007.

[27] N. Saito, "The generalized spike process, sparsity and statistical independence," in *Modern Signal Processing*. Cambridge University Press, 2002, pp. 317–340.

[28] H. Wickham, "Tidy data," *Journal of Statistical Software*, vol. 59, no. 10, p. 1–23, 2014.

[29] D. I. Shuman, C. Wiesmeyr, N. Holighaus, and P. Vandergheynst, "Spectrum-adapted tight graph wavelet and vertex-frequency frames," *IEEE Transactions on Signal Processing*, vol. 63, pp. 4223–4235, 2013.

[30] T. Wise, L. Marwood, A. Perkins, A. Herane-Vives, R. Joules, D. Lythgoe, W.-M. Luh, S. Williams, A. Young, A. Cleare, and D. Arnone, "Instability of default mode network connectivity in major depression: a two-sample confirmation study," *Translational Psychiatry*, vol. 2017, p. e1105, 2017.

[31] M. Pawlak, S. Bray, and D. Kopala-Sibley, "Resting state functional connectivity as a marker of internalizing disorder onset in high-risk youth," *Scientific Reports*, vol. 12, 2022.